Available online at www.sciencedirect.com

ScienceDirect

Proceedings of the Combustion Institute 38 (2021) 6521–6531

Proceedings of the Combustion Institute

www.elsevier.com/locate/proci

Kinetic study of plasma-assisted n-dodecane/O_2/N_2 pyrolysis and oxidation in a nanosecond-pulsed discharge

Hongtao Zhong [a], Xingqian Mao [a,*], Aric C Rousso [a], Charles L Patrick [b], Chao Yan [a], Wenbin Xu [a], Qi Chen [c], Gerard Wysocki [b], Yiguang Ju [a]

[a] *Department of Mechanical and Aerospace Engineering, Princeton University, Princeton, NJ 08544, USA*
[b] *Department of Electrical Engineering, Princeton University, Princeton, NJ 08544, USA*
[c] *School of Mechanical, Electronic and Control Engineering, Beijing Jiaotong University, Beijing 100044, China*

Received 8 November 2019; accepted 28 June 2020
Available online 31 August 2020

Abstract

The present study investigates the kinetics of low-temperature pyrolysis and oxidation of n-dodecane/O_2/N_2 mixtures in a repetitively-pulsed nanosecond discharge experimentally and numerically. Time-resolved TD-LAS measurements, steady-state gas chromatography (GC) sampling, and mid-IR dual-modulation Faraday rotation spectroscopy (DM-FRS) measurements are conducted to quantify temperature as well as species formation and evolution. A plasma-assisted n-dodecane pyrolysis and oxidation kinetic model incorporating the reactions involving electronically excited species and NO_x chemistry is developed and validated. The results show that a nanosecond discharge can dramatically accelerate n-dodecane pyrolysis and oxidation at low temperatures. The numerical model has a good agreement with experimental data for the major intermediate species. From the pathway analysis, electronically excited N_2^* plays an important role in n-dodecane pyrolysis and oxidation. The results also show that with addition of n-dodecane, NO concentration is reduced considerably, which suggests that there is a strong NO kinetic effect on plasma-assisted low-temperature combustion via NO-RO_2 and NO_2-fuel radical reaction pathways. This work advances the understandings of the kinetics of plasma-assisted low-temperature fuel oxidation in N_2/O_2 mixtures.

Keywords: Plasma-assisted combustion; Low-temperature chemistry; Nanosecond pulsed discharge; Laser diagnostics; N-Dodecane/O_2/N_2 mixture

1. Introduction

Fuel pyrolysis and oxidation activated by non-equilibrium plasma discharges have recently received great attention in advanced engines and fuel reforming [1] as it provides new reaction

* Corresponding author.
E-mail address: xingqian@princeton.edu (X. Mao).

https://doi.org/10.1016/j.proci.2020.06.016
1540-7489

pathways for ignition control and selective chemical synthesis. Previous studies have shown that non-equilibrium plasma can kinetically enhance combustion through electron-impact molecular dissociation, excitation, ionization as well as plasma-assisted low-temperature reactions. Specifically, the nanosecond pulsed discharge (NSD), with ultrafast (≤ 1 ns) voltage rise and energy input, generates high reduced electric field (E/N, where E is the electric field strength and N is the gas number density), increases electron temperatures and therefore has a promising kinetic effect on combustion reactions via volumetric production of excited species. NSD provides an ideal platform to study the kinetic effects from plasma and develop plasma assisted combustion (PAC) kinetic mechanisms.

Previous kinetic studies using NSD have been conducted mostly on simple fuels including small hydrocarbons [2,3] with the dilution of helium or argon. The modeling results matched relatively well with the measurements and showed significant kinetic enhancement from plasma-generated species like e, O, O(^{1}D), Ar* and He* on the ignition behavior. However, most real-world combustion systems use air as the oxidizer. The presence of N_2 and O_2 increases the complexity of PAC reaction pathways due to vibrational and electronic excitation of nitrogen and NO_x formation, but it brings more possible kinetic couplings for low-temperature fuel pyrolysis and oxidation processes. Thus, one fundamental question limiting PAC applications in real engine environment is: what is the kinetic mechanism of plasma assisted combustion of practical fuels in air?

Our recent plasma-assisted kinetics studies on n-pentane with He dilution [4] and n-heptane with Ar dilution [5] have shown that plasma dramatically accelerated the fuel oxidation at low temperature. However, *in situ* species diagnostics also revealed that the kinetic model failed to predict the time-dependent profiles of even major species due to the lack of appropriate understanding of plasma reaction kinetics for large alkanes [5]. By updating the missing pathways of electron-impact reactions in n-pentane pyrolysis, the kinetic mechanism dramatically improved the model prediction, even when tested on the oxidative case. The next step, therefore, is to study larger representative jet fuel components, like n-dodecane, which represent use cases where these plasma-assisted reactions may play a role in enhancement [6].

The present paper aims to study the plasma-assisted fuel pyrolysis and oxidation of n-dodecane with nitrogen dilution. A total pressure of 30 Torr is used to ensure the homogeneity of the plasma discharge. In the engine environment, the plasma may interact with liquid fuels in affecting vaporization. However, fuel pyrolysis and oxidation mainly take place in the gas phase. While the low-pressure conditions may not be representative of real engine pressures, the elementary plasma chemistry coupled with electron impact reactions is a function of the reduced electric field (E/N) and the electron energy, where N indicates the effects of temperature and pressure. Therefore, by matching E/N correctly, the present kinetic mechanism can be extended to higher temperatures and pressures. Certainly, under high temperatures and pressures, plasma instability could play a role and plasma begins to transit from homogeneous to filamentary [7]. In that case, the kinetic mechanism is still valuable for understanding the effect of fast and slow heating by plasma.

The paper is structured as the followings: First, time-dependent TDLAS measurements, steady-state GC sampling and DM-FRS measurements are performed to quantify fuel, intermediate species and NO evolution in plasma-assisted fuel pyrolysis and oxidation of $C_{12}H_{26}/O_2/N_2$ mixtures. Second, a plasma combustion kinetic model of n-dodecane incorporating N_2^*, O(^{1}D), O(^{1}S) as well as N an NO_x with n-dodecane and fuel radicals is developed and validated. Then, the numerical modeling results of reactants, intermediate species and products are compared with experimental measurements. Path flux analysis is conducted to understand the key reaction pathways. The importance of plasma generated species as well as NO_x is identified. The effects of electron impact reactions of n-dodecane on intermediate species formation in plasma-assisted fuel oxidation are discussed. Finally the effects of N and NO_x on n-dodecane pyrolysis and oxidation are studied.

2. Experimental method

The reactor for this study, seen in Fig. 1, is a rectangular quartz flow reactor. Two electrodes (45 × 45 mm) are attached to the top and bottom of the cell to form a dielectric barrier discharge (DBD). A nanosecond-pulsed power supply (FID GmbH FPG 30-50MC4) is used for plasma generation, with a maximum repetition frequency of 30 kHz, FWHM of 12 ns, and maximum peak voltage of 32 kV, which is operated in both continuous and burst modes via an external digital pulse generator (SRS DG535). The burst mode is utilized for all time-dependent measurements with a total burst of 450–600 pulses at 30 kHz, and a total discharge time of 0.015–0.02 s. The reactor is kept at 30 Torr, with an overall flow velocity of 0.5 m/s. The burst frequency is 1 Hz. A delay of 0.98–0.985 s between bursts is used for gas replenishment. A syringe pump and a liquid vaporizer are coupled to the upstream of the reactor to provide gaseous n-dodecane. Due to n-dodecane's high boiling point (489.45 K), all lines must be heated to prevent condensation and maintain accurate fuel concentration. 1% n-dodecane and 99% N_2 in the pyrolysis case and 1% n-dodecane, 19% oxygen and 80% N_2 in the oxidative case are supplied into the sys-

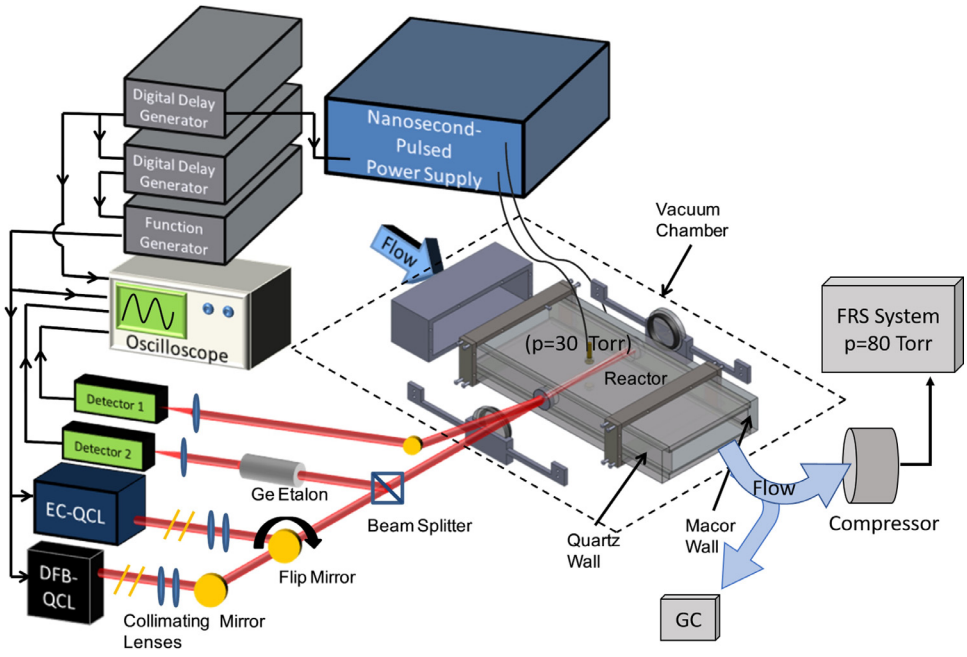

Fig. 1. Experimental setup.

tem, respectively. During the discharge, single-shot ICCD images (Princeton Instruments PI-MAX) of individual pulses within the burst are taken to confirm uniformity (Typical ICCD images are in Supplementary materials). In the pyrolysis case, the plasma keeps homogeneous with the increase of total burst pulses due to endothermic fuel decomposition reactions. The final total burst count is 600 to allow for adequate fuel decomposition but avoid excessive heating from plasma. In the oxidative case, the pulse count within a burst is held at 450, as an increase of intensity and narrowing of the plasma discharge are seen at the edges of the plasma with increasing numbers of pulses.

For *in-situ* measurements of species-time profiles, a 24-pass Herriott multi-pass cell is built into the walls of the reactor and utilized for mid-IR tunable diode laser absorption spectroscopy (TDLAS) measurements. From the NIST database, an absorption line at 1377 cm^{-1} is chosen for n-dodecane, which requires calibration measurements due to its broadband absorption profile in the mid-IR. A separate, heated quartz cylindrical flow tube is used for n-dodecane absorption cross section calibration measurements (More details are in Supplementary materials). Time-resolved signals of other species are also quantified by direct absorption. Quantification of CH_4 is at 1341.62 cm^{-1}, C_2H_2 is at 1342.35 cm^{-1}, and H_2O is at both 1338.55 cm^{-1} and 1339.15 cm^{-1}, which can be further utilized for the two-line temperature measurements [8]. The above measurements all utilize a Continuous Wave External Cavity Mode Hop Free (CW-EC-MHF) QCL from Daylight Solutions. CH_2O is quantified at 1726.79 cm^{-1} using a DFB-QCL from Alpes Lasers (sbcw3176). The scan rate of all lasers is monitored using a 50.8 mm Germanium etalon (FSR 0.74 GHz at 1345 cm^{-1}) and data is recorded on a Tektronix DPO 7104C oscilloscope. All data sets are averaged over 25 runs, utilizing the fitting of temperature to determine line broadening parameters, and demonstrating very high repeatability. The uncertainty of the temperature measurements is ±10 K at 300 K. The uncertainty for the n-dodecane concentration measurements is within ±20%, mainly based on run to run fluctuations in the calibration process. The uncertainty of other species concentrations is estimated as ±5%, which is originated from spatial intensity non-uniformities in the plasma, electronic interferences between NSD and the detector, and the fitting of the spectral line shape.

For steady-state measurements, a quartz sampling probe is inserted downstream of the plasma discharge. Samples are analyzed using a gas chromatograph (GC) (TCD; Inficon 3000), with uncertainties of ±5% of the measured concentrations, which can provide additional validation targets for the kinetic mechanism. A dual modulation FRS (DM-FRS) system [9,10] is applied to detect steady-state nitric oxide (NO) concentrations during the continuous bursts of the NSD. Faraday rotation spectroscopy measures the rotation of polarization of light induced by circular birefrin-

gence from the Zeeman-split transitions of paramagnetic gaseous species (e.g. NO, OH, HO_2, etc.) subjected to an external magnetic field. FRS enables reliable quantitative concentration measurements of paramagnetic species in the presence of spectrally-interfering diamagnetic molecules including H_2 and CO_2, which are formed promptly in the combustion environment. The DM-FRS system targets P(19/2)e doublet transition at 1842.946 cm^{-1} of the reactive mixture from the reactor. The pressure is stabilized at 80 Torr with a flow rate of 20 sccm. The system was constructed by Zhang et al. [9] and Wang et al. [10]. Modulation of both the laser current and the applied magnetic field provides laser intensity independent and etalon-free measurements.

3. Numerical method and kinetic model

The numerical modeling is conducted by a zero-dimensional hybrid ZDPlasKin-CHEMKIN model which was developed and validated in previous works [11,12]. The model incorporates the plasma kinetics solver ZDPlasKin [13] and the combustion kinetics solver CHEMKIN II [14] by a splitting method. The discharge voltage measured is used as input to calculate the *E*/*N* in the plasma and has been described in detail in [11]. The voltage and *E*/*N* of a single pulse can be found in the Supplementary materials.

A plasma-assisted n-dodecane combustion mechanism is developed in this work (see Supplementary materials for reaction details). The mechanism consists of both plasma and combustion kinetic sub-mechanisms. The combustion submechanism is reduced from Cai's model [15] to 141 species and 632 reactions by Princeton CHEM-RC [16]. The C0-C2 chemistry is replaced by HP-Mech [17] for accurate modeling the low temperature chemistry. The reactions of N and NO_x with fuel and fuel radicals are adapted from [18–20]. The plasma mechanism incorporates the reactions of electronically excited species $O_2(a^1\Delta_g)$, $O_2(b^1\Sigma_g^+)$, O_2^*, $O(^1D)$, $O(^1S)$, $N_2(A)$, $N_2(B)$, $N_2(a')$, N_2 (C) and $N(^2D)$; charged species N_2^+ and O_2^+; and electron. The final mechanism consists of 198 species, 239 reactions in the plasma mechanism and 1128 reactions in the combustion mechanism. The rotationally and vibrationally excited species are considered to provide the gas heating by relaxation. As the experiments are conducted at the highly diluted conditions and the *E*/*N* in this study is 400–600 Td, most electron energy goes to the excitation of N_2 and O_2. Due to the fact that cross sections between electrons with n-dodecane are unavailable and the electron-impact n-dodecane dissociation reactions are less important compared with other electron energy consumption pathways (shown in Supplementary materials), it is originally assumed that the fuel is mainly consumed by the electronically excited N_2^* ($N_2(A)$, $N_2(B)$, $N_2(a')$ and $N_2(C)$) in the pyrolysis condition and additional contribution by $O(^1D)$ and $O(^1S)$ in the oxidation condition. Note that with 99% N_2 concentration in pyrolysis condition, $N_2(B)$ and $N_2(C)$ mainly transit into $N_2(A)$ and $N_2(a')$ through reactions $N_2(B) + N_2 \longrightarrow N_2(A) + N_2$, $N_2(C) \longrightarrow N_2(B)$ and $N_2(C) + N_2 \longrightarrow N_2(a') + N_2$. Even with O_2 addition in the oxidation case, due to the fast reaction rates between N_2(B, C) and O_2 [21], fuel consumption from these two species can be neglected. Therefore, the n-dodecane consumption by N_2^* can be simplified by $N_2(A)$ and $N_2(a')$. The C–C and C–H bond energies of n-dodecane are 3.7 eV [22] and 4.1–4.3 eV [23] respectively, while the potential energies of $N_2(A)$ and $N_2(a')$ are 6.17–7.8 eV and 8.4–8.89 eV, respectively. Therefore, $N_2(A)$ can break two C–C bonds and $N_2(a')$ can break up to two C–C or C–H bonds. The reactions between $O(^1D)$ and n-dodecane can either be an H-abstraction reaction to form OH and fuel radical or an insertion into C–H bond to form CH_2O [24]. Similar reactions are considered for $O(^1S)$. Based on the above analysis, the rate constants and branching ratios for reactions between $N_2(A)$, $N_2(a')$, $O(^1D)$ and $O(^1S)$ and n-dodecane are estimated based on fitting with experimental data and sensitivity analysis.

4. Results and discussion

4.1. TDLAS results

Fig. 2 shows the time-dependent temperature measured and fitted profiles of n-dodecane pyrolysis and oxidation. In the pyrolysis case, CH_4 is used for the two-line temperature measurements but does not have enough production until approximately halfway through the burst. Therefore, temperature measurements begin at 10 ms. In the oxidative case, H_2O is used for two-line measurements, which is produced more promptly and facilitates temperature measurements starting from 3 ms. A baseline thermocouple temperature measurement of the reactor, taken without plasma operation, is shown as the dotted horizontal line. The temperature rise in the pyrolysis is mainly caused by plasma Joule heating. With O_2 addition, there is an additional $\sim$60 K temperature rise caused by fuel oxidation even with fewer plasma pulses. The measured temperature profiles are used as input for kinetic modeling.

Fig. 3 shows the measurement and modeling of n-dodecane pyrolysis and oxidation during and after the plasma bursts. 20% of the fuel is consumed during the plasma burst in the pyrolysis case. The model agrees well with the experimental data overall. Only a small discrepancy exists at the end but still within the measurement error. This small fluctuations in the signal may result from either phys-

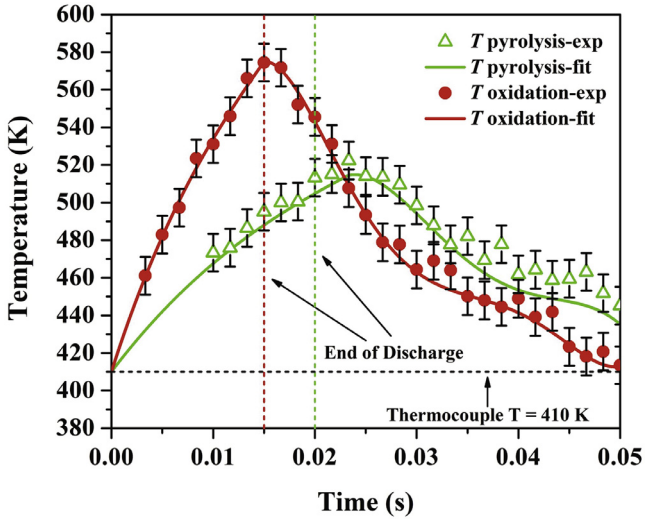

Fig. 2. Temperature during and after the 30 kHz plasma burst for the pyrolysis, oxidative, and without plasma conditions. The fitting used by the model is shown by the solid lines.

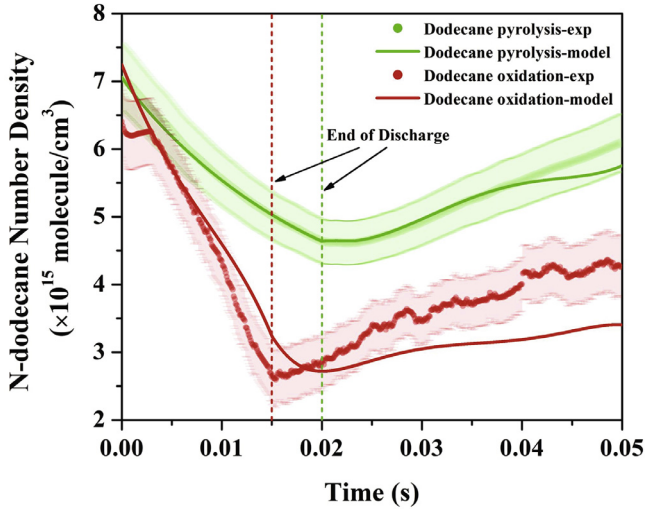

Fig. 3. Time-dependent measurements and model predictions of n-dodecane consumption for a 0.01/0.99 mixture of $C_{12}H_{26}/N_2$ and 0.01/0.19/0.80 mixture of $C_{12}H_{26}/O_2/N_2$.

ical vibrations captured by the measurements or beam steering due to the great temperature change in this experiment. In the oxidative case, the decay trend with over 60% fuel consumption is captured fairly well. However, the absolute difference in number density is observed. This difference may be caused by two factors. First, the model underpredicts the number densities of major products during the plasma bursts and shows a better agreement with the experimental measurement in the later stage after the bursts, which will be discussed later. This leads to the predicted n-dodecane number density decreasing slower and reaching minimum later than the experimental measurement after the bursts. Second, this difference may also be due to the generation of more intermediate species and their interference with the laser absorption at 1377 cm^{-1}. The error on this measurement is approximately $\pm 20\%$, due to laser drift, accuracy of calibrated n-dodecane cross sections, and spatial nonuniformities near the mirrors.

Fig. 4 shows the time-dependent CH_4 and C_2H_2 number densities in the pyrolysis condition. Together with the steady state measurements, the

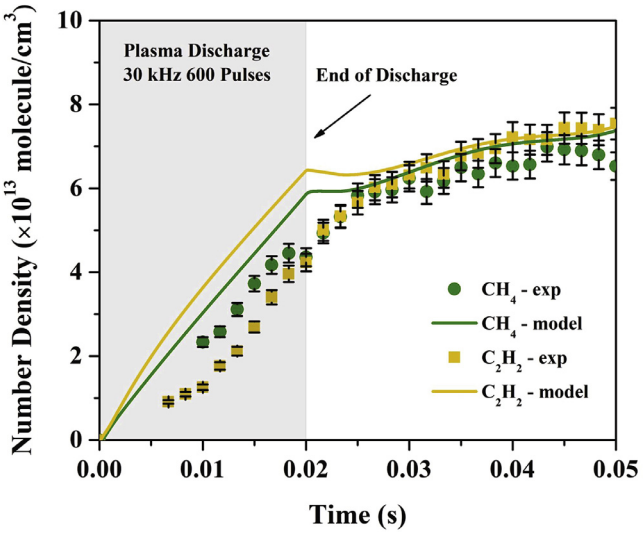

Fig. 4. Time evolution of CH_4 and C_2H_2 with model predictions for the pyrolysis case (0.01 $C_{12}H_{26}$/0.99 N_2).

species concentrations are utilized to determine the reaction channels and branching ratios between N_2(A, a′) with fuels. The modeling results predict the pyrolysis species fairly accurately after the plasma bursts. The path flux analysis is conducted by integrating the time duration of 0.05 s. Fig. 5 shows that n-dodecane is dissociated by N_2(A) (61.4%) and N_2(a′) (24%) to produce small hydrocarbons directly or fuel radicals, as well as by H-abstraction reaction (14.6%) to produce H_2 and $C_{12}H_{25}$. The plasma generated fuel radicals are consumed to produce H_2 and C1–C3 hydrocarbons, and 66% of them recombine to form n-dodecane again.

In the oxidation condition, as shown in Fig. 3, the fuel consumption increases dramatically with fewer pulses. Besides the dissociation effect to fuel, 59% of N_2^* is quenched by O_2 to generate O, O(^{1}D) and O(^{1}S). The path flux analysis in Fig. 5 shows that $C_{12}H_{26}$ consumed by N_2(A, a′) and O(^{1}D, ^{1}S) accounts for 3.5% and 6.1% of the total fuel consumption, contributing to the production of fuel radicals and CH_2O. The n-dodecane consumption by OH and O becomes the dominate pathways for fuel consumption, accounting for 65.3% and 23% respectively for the time-dependent condition. The O radical produced in the plasma promotes the H-abstraction reaction of n-dodecane to form $C_{12}H_{25}$ and OH, and OH further accelerates the fuel consumption. Fig. 5 shows that the production of $C_{12}H_{25}$ triggers a cycle to OH production and fuel consumption. $C_{12}H_{25}O_2$ is produced by an addition reaction of $C_{12}H_{25}$ and O_2. The isomerization of $C_{12}H_{25}O_2$ leads to $C_{12}H_{24}OOH$ formation. Then, the decomposition of $C_{12}H_{24}OOH$ produces $C_{12}H_{24}O$ and OH radicals.

The model also predicts the H_2O time profiles (shown in Fig. 6) reasonably well, up to 90% of which is produced from $C_{12}H_{26}$ + OH. However, there is an under-prediction for CH_2O number density. Given previous studies [1], CH_2O may be generated directly from low-temperature reactions involving hydroperoxy alkyl radicals O_2QOOH. However, the current model fails to include such complicated low-temperature kinetic pathways, which may lead to differences in CH_2O number densities.

4.2. Steady-state GC results

The kinetic model is also applied to simulate steady-state GC measurements. In the pyrolysis case, measured species match relatively well with the simulation under different discharge frequencies (shown in Fig. 7).

In the oxidation case, even though the primary oxidative products (H_2O, CH_2O, CO, and CO_2) with high concentrations from the modeling match well with the experimental measurements, the C0–C5 hydrocarbons with low concentrations are all under-predicted (shown in Fig. 8). From pathway analysis, in the current model, most radicals forming these small hydrocarbons are consumed by O and O_2 in the oxidation conditions. However, these species may also be produced directly from electron-impact dissociation or ionization reactions of n-dodecane, which were not taken into account originally. Similar with the analysis in our previous kinetic studies of pentane [4], one more case is conducted by adding the estimated electron-impact reactions with n-dodecane. The cross sections are adjusted by using the available cross sections of C_2H_6 [25] as reference. The result shows

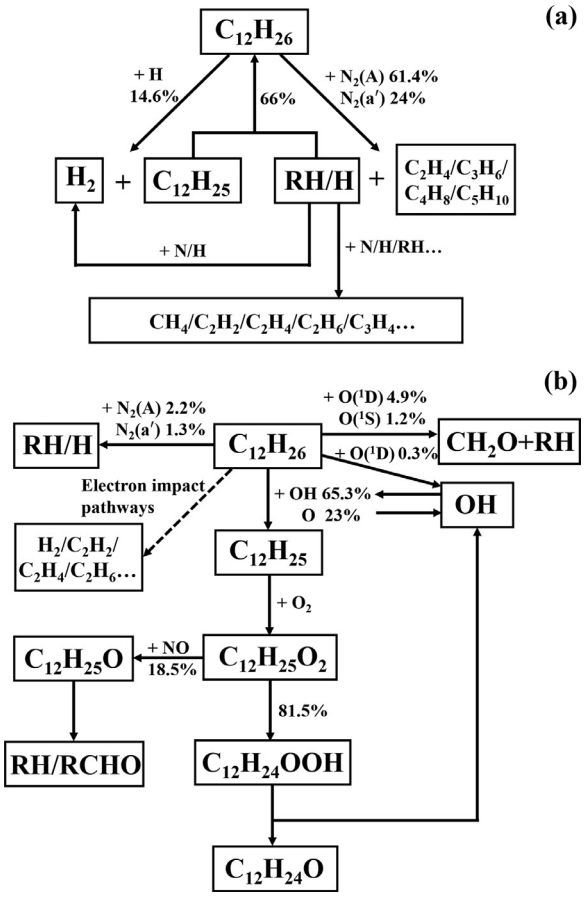

Fig. 5. Path flux of fuel in the time-dependent simulations for the (a) pyrolysis and (b) oxidation condition. All percentages do not sum to 100%, as other reactions add small quantities to the total. (R is the fuel radical).

that such electron impact reactions do improve the modeling prediction for small hydrocarbons production, as shown in Fig. 8. This indicates that the accurate branching ratios and cross sections of electron impact reactions for large hydrocarbons are critical and dedicated measurements and quantum calculation for electron-impact dissociation and ionization reactions are required for future plasma-assisted kinetic studies.

4.3. Steady-state DM-FRS NO results

NO is one of the most active species produced in N_2/O_2 plasma discharge [21]. To further investigate possible kinetic couplings between plasma-assisted low-temperature combustion and NO_x chemistry generated by N_2/O_2 discharge, a DM-FRS system is used to quantify NO concentrations *ex situ*. The measurements together with the model predictions are shown in Fig. 9. Compared with the baseline NO measurements in the 0.8 N_2/0.2 O_2 mixture, the presence of 1% fuel significantly inhibits the final NO yield in the mixture (lower than 3 ppm). Moreover, with higher discharge frequency and hence higher plasma energy deposition, such NO reduction effect is more prominent.

To further understand the kinetic effects of fuels on NO_x chemistry, path flux analysis is performed for nitrogen element. Given the experimental conditions of temperature (375–575 K) and pressure (30 Torr), N and $N(^2D)$ produced by $e + N_2 \longrightarrow e + N + N(^2D)$, $e + N_2^+ \longrightarrow N + N(^2D)$ and $e + N_2^+ \longrightarrow N + N$ are two of the major radicals in the plasma with a peak *E*/*N* of 400–600 Td. Based on the model, in the pyrolysis condition (shown in Fig. 10(a)), reactions between N and fuel radicals (CH_2, CH_3, and C_2H_5) promote the production of H, NH and C_2H_4. Reaction $H + NH = H_2 + N$ becomes a major pathway for H_2 production besides $CH_2 + H = CH + H_2$ and $C_{12}H_{26} + H = C_{12}H_{25} + H_2$. In the oxidation condition (shown in Fig. 10(b)), N and $N(^2D)$ promote the O, NO and $O(^1D)$ production via $N + O_2 = NO + O$, $N(^2D) + O_2 \longrightarrow NO + O(^1D)$ and $N(^2D) + O_2 \longrightarrow NO + O$.

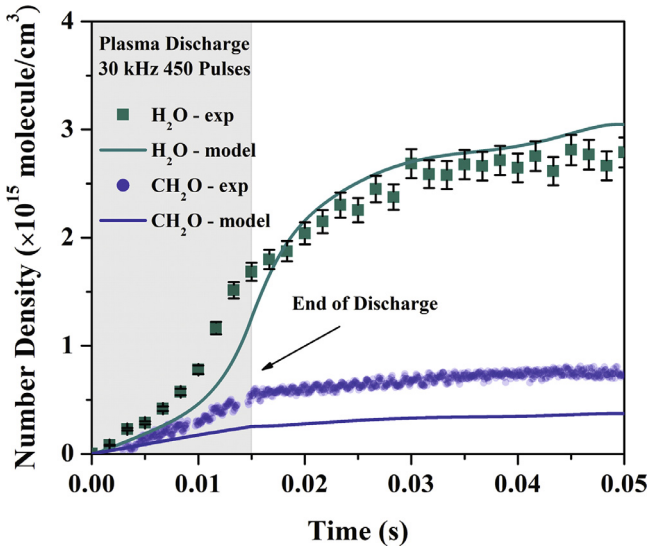

Fig. 6. TDLAS time evolution of H_2O and CH_2O with model predictions for the oxidation case (0.01 $C_{12}H_{26}$/0.19 O_2/0.80 N_2).

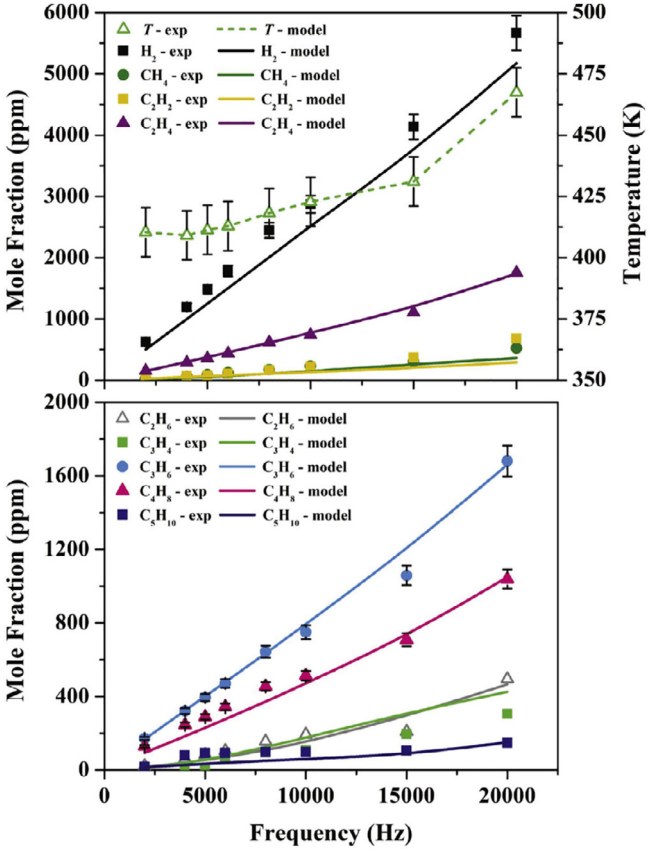

Fig. 7. Steady-state GC pyrolysis measurements of (Up) temperature and small hydrocarbon species and (Down) large hydrocarbon species for 0–20 kHz continuous plasma pulse frequencies for 0.01 $C_{12}H_{26}$/0.99 N_2.

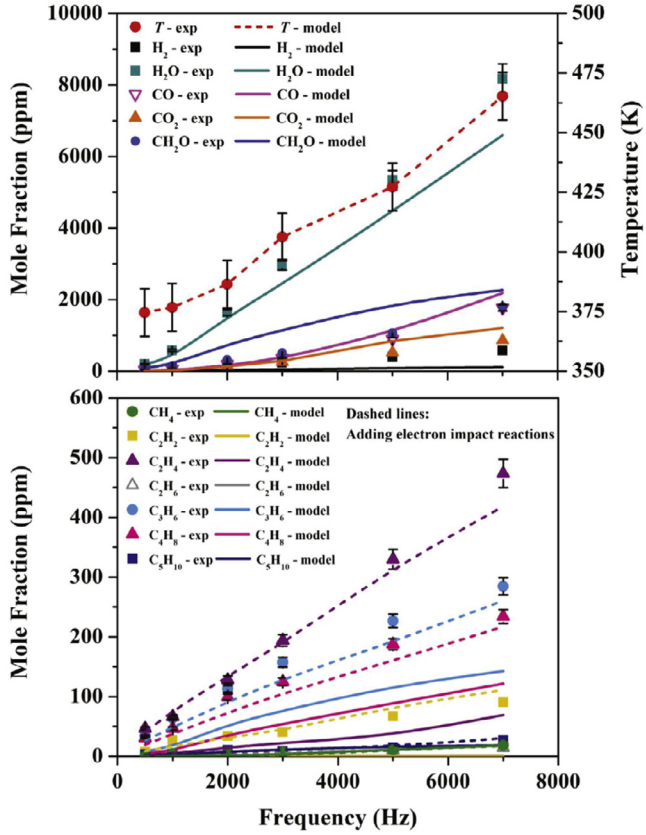

Fig. 8. Steady-state GC oxidation measurements of (Up) temperature and small species and (Down) hydrocarbon species for 0–7 kHz continuous plasma pulse frequencies for 0.01 $C_{12}H_{26}$/0.19 O_2/0.80 N_2.

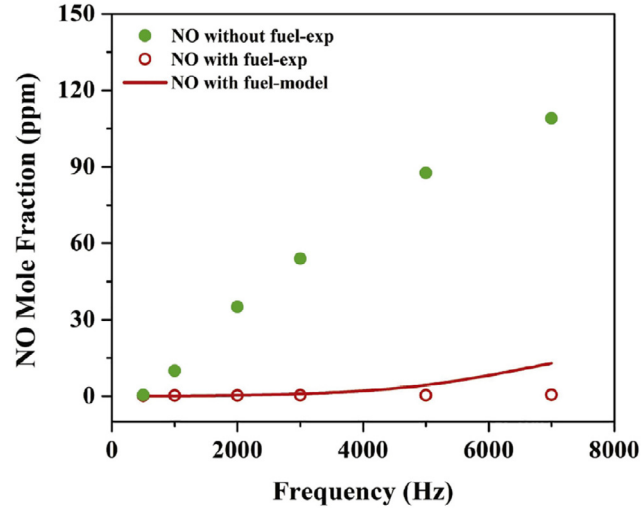

Fig. 9. Steady-state DM-FRS NO measurements for 0–7 kHz continuous plasma pulse frequencies for 0.80 N_2/0.20 O_2 and 0.01 $C_{12}H_{26}$ /0.19 O_2/0.80 N_2.

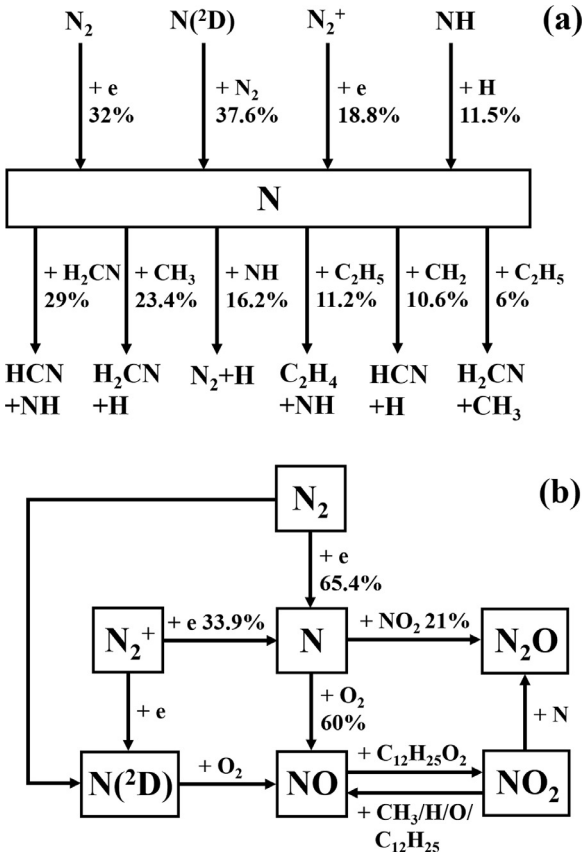

Fig. 10. Path Flux of nitrogen element for the (a) pyrolysis and (b) oxidation condition. All percentages do not sum to 100%, as other reactions add small quantities to the total.

From the above analysis, the formation of N and NO in the presence of fuel is still governed by N_2-O_2 chemistry. However, NO consumption pathways are shifted in the presence of fuel. Without hydrocarbons, NO consumption is mainly through third-body reaction NO + O(+M) = NO_2(+M) in the kinetic model, which is consistent with previous studies [26]. The product NO_2 could also be eliminated by reverse reaction NO_2 + O = NO + O_2. With hydrocarbons, NO to NO_2 oxidation is greatly enhanced as the fuel species goes through low temperature oxidation and generates a large amount of alkylperoxy radicals (e.g. $C_{12}H_{25}O_2$) which act as an efficient converter from NO to NO_2. In the kinetic model, 92% of NO is consumed by the reactions with $C_{12}H_{25}O_2$ forming $C_{12}H_{25}O$ and NO_2, which has a large path flux shown in Fig. 10. Then reactions between NO_2 and fuel radicals (H, CH_3 and $C_{12}H_{25}$) continue producing active radicals including OH, CH_3O, $C_{12}H_{25}O$ and NO, accounting for 72% of the total NO_2 consumption. The above discussion demonstrates NO has a strong catalytic effect on the low temperature fuel oxidation via NO-RO_2 and NO_2-fuel radical reaction pathways [18].

5. Conclusions

The plasma-assisted low-temperature n-dodecane pyrolysis and oxidation kinetics in N_2/O_2 using a nanosecond repetitively-pulsed DBD discharge were studied with time-dependent TDLAS *in situ* measurements, steady-state GC sampling and *ex situ* DM-FRS measurements in a plasma flow reactor. A new plasma-assisted kinetic model was developed and validated against the measured data. The modeling results show that the kinetic model can predict the experimental data well for the pyrolysis condition and major species in the fuel oxidation condition. The under-prediction of low-concentration small hydrocarbons in the oxidation condition suggests that electron impact reactions also contribute to species production in high N_2 diluted mixtures. The path flux results show that the major pyrolysis pathway for n-dodecane is the dissociation reaction by electronically excited N_2(A) and N_2(a′). One-third of the fuel radicals recombine to generate small hydrocarbons and the rest of them recombine back to n-dodecane. In the oxidation condition, the n-dodecane is primarily consumed by O and OH. Specifically,

O generated in plasma promotes the production of OH and $C_{12}H_{25}$, and accelerates the production of OH via $C_{12}H_{25} + O_2 \longrightarrow C_{12}H_{25}O_2 \longrightarrow C_{12}H_{24}OOH \longrightarrow C_{12}H_{24}O + OH$. High concentration of N and $N(^2D)$ contributes to H, NH and C_2H_4 production in the pyrolysis condition, as well as NO production in the oxidation condition. The results show that significant amount of NO is produced in a N_2/O_2 plasma. However, with the addition of n-dodecane, the concentration dramatically decreases via NO and $C_{12}H_{25}O_2$ reaction to form $C_{12}H_{25}O$ and NO_2. Meanwhile, reactions between NO_2 and H, CH_3 and $C_{12}H_{25}$ produce alkoxy radicals and NO. These plasma-assisted NO reaction pathways will significantly modify the plasma-assisted fuel oxidation at low temperatures.

Declaration of Competing Interest

The authors declare that they have no known competing financial interests or personal relationships that could have appeared to influence the work reported in this paper.

Acknowledgments

This work was supported by NSF grant CBET 1903362, DOE NETL grant DE-FE0026825, and DOE grant DE-SC0020233 of Plasma Science Center.

Supplementary material

Supplementary material associated with this article can be found, in the online version, at doi:10.1016/j.proci.2020.06.016.

References

[1] Y. Ju, W. Sun, *Progr. Energy Combust. Sci.* 48 (2015) 21–83.
[2] J.K. Lefkowitz, P. Guo, A. Rousso, Y. Ju, *Philos. Trans. R. Soc. A: Math. Phys. Eng. Sci.* 373 (2048) (2015) 20140333.
[3] M.A. Boumehdi, S.A. Stepanyan, P. Desgroux, G. Vanhove, S.M. Starikovskaia, *Combust. Flame* 162 (4) (2015) 1336–1349.
[4] A. Rousso, X. Mao, Q. Chen, Y. Ju, *Proc. Combust. Inst.* 37 (4) (2019) 5595–5603.
[5] A. Rousso, S. Yang, J. Lefkowitz, W. Sun, Y. Ju, *Proc. Combust. Inst.* 36 (3) (2017) 4105–4112.
[6] T. Yao, Y. Pei, B.-J. Zhong, S. Som, T. Lu, K.H. Luo, *Fuel* 191 (2017) 339–349.
[7] S. Shcherbanev, C. Ding, S. Starikovskaia, N. Popov, *Plasma Sour. Sci. Technol.* 28 (6) (2019) 065013.
[8] A. Farooq, J.B. Jeffries, R.K. Hanson, *Meas. Sci. Technol.* 19 (7) (2008) 075604.
[9] E.J. Zhang, B. Brumfield, G. Wysocki, *Opt. Exp.* 22 (13) (2014) 15957–15968.
[10] Y. Wang, M. Nikodem, G. Wysocki, *Opt. Exp.* 21 (1) (2013) 740–755.
[11] X. Mao, Q. Chen, A.C. Rousso, T.Y. Chen, Y. Ju, *Combust. Flame* 206 (2019) 522–535.
[12] X. Mao, A. Rousso, Q. Chen, Y. Ju, *Proc. Combust. Inst.* 37 (4) (2019) 5545–5552.
[13] S. Pancheshnyi, B. Eismann, G. Hagelaar, L. Pitchford, *Bull. Am. Phys. Soc.* 53 (2008).
[14] R.J. Kee, F.M. Rupley, J.A. Miller, Chemkin-II: A Fortran chemical kinetics package for the analysis of gas-phase chemical kinetics, *Technical Report*, Sandia National Labs., Livermore, CA (USA), 1989.
[15] L. Cai, H. Pitsch, S.Y. Mohamed, V. Raman, J. Bugler, H. Curran, S.M. Sarathy, *Combust. Flame* 173 (2016) 468–482.
[16] W. Sun, Z. Chen, X. Gou, Y. Ju, *Combust. Flame* 157 (7) (2010) 1298–1307.
[17] X. Yang, X. Shen, J. Santner, H. Zhao, Y. Ju, *Princeton HP-Mech.* (2017) http://engine.princeton.edu/mechanism/HP-Mech.html.
[18] H. Zhao, L. Wu, C. Patrick, Z. Zhang, Y. Rezgui, X. Yang, G. Wysocki, Y. Ju, *Combust. Flame* 197 (2018) 78–87.
[19] P. Gokulakrishnan, C.C. Fuller, M.S. Klassen, *J. Eng. Gas Turb. Power* 140 (4) (2018).
[20] J. Anderlohr, R. Bounaceur, A.P. Da Cruz, F. Battin-Leclerc, *Combust. Flame* 156 (2) (2009) 505–521.
[21] M. Capitelli, C.M. Ferreira, B.F. Gordiets, A.I. Osipov, *Plasma Kinetics in Atmospheric Gases*, 31, Springer Science & Business Media, 2013.
[22] Y.-R. Luo, *Handbook of Bond Dissociation Energies in Organic Compounds*, CRC Press, 2002.
[23] Q.-D. Wang, J.-B. Wang, J.-Q. Li, N.-X. Tan, X.-Y. Li, *Combust. Flame* 158 (2) (2011) 217–226.
[24] X. Yang, *Phys. Chem. Chem. Phys.* 8 (2) (2006) 205–215.
[25] L. Pitchford, B. McKoy, A. Chutjian, S. Trajmar, in: Proceedings of the Meeting of the Fourth International Swarm Seminar and the Inelastic Electron-Molecule Collisions Symposium, Springer-Verlag, New York, 1987. July 1923, 1985
[26] A. Khacef, J.M. Cormier, J.M. Pouvesle, *J. Phys. D: Appl. Phys.* 35 (13) (2002) 1491.